This article has been accepted for publication in a future issue of this journal, but has not been fully edited. Content may change prior to final publication. Citation information: DOI 10.1109/TUFFC.2017.2786300, IEEE Transactions on Ultrasonics, Ferroelectrics, and Frequency Control

Realistic Vendor-Specific Synthetic Ultrasound Data for Quality Assurance of 2D Speckle Tracking Echocardiography: Simulation Pipeline and Open Access Database.

Martino Alessandrini*, Bidisha Chakraborty, Brecht Heyde, Olivier Bernard, Mathieu De Craene, Maxime Sermesant and Jan D'hooge.

***Abstract*—Two dimensional (2D) echocardiography is the modality of choice in the clinic for the diagnosis of cardiac disease. Hereto, speckle tracking (ST) packages complement visual assessment by the cardiologist by providing quantitative diagnostic markers of global and regional cardiac function (e.g. displacement, strain, strain-rate). Yet, the reported high vendor-dependency between the outputs of different ST packages raises clinical concern and hampers the widespread dissemination of the ST technology. In part, this is due to the lack of a solid commonly accepted quality assurance pipeline for ST packages.**

Recently, we have developed a framework to benchmark ST algorithms for three dimensional (3D) echocardiography by using realistic simulated volumetric echocardiographic recordings. Yet, 3D echocardiography remains an emerging technology while the compelling clinical concern is, so far, directed to the standardization of 2D ST only.

By building upon our previous work, we present therefore in this paper a pipeline to generate realistic synthetic sequences for 2D ST algorithms. Hereto, the synthetic cardiac motion is obtained from a complex electro-mechanical heart model while realistic vendor-specific texture is obtained by sampling a real clinical ultrasound recording. By modifying the parameters in our pipeline, we generated an open access library of 105 synthetic sequences encompassing i) healthy and ischemic motion patterns, ii) most common apical probe orientations iii) vendor specific image quality from 7 different systems. Ground truth deformation is also provided to allow performance analysis. The application of the provided data-set is also demonstrated in the bench-marking of a recent academic ST algorithm.

I. Introduction

SPECKLE tracking echocardiography (STE) is available clinically to image cardiac displacement and strain non-invasively at an adequate temporal resolution. Clinical feasibility of STE derived strain has been shown in many studies: strain has been used to diagnose myocardial ischaemia; it has been proposed as a tool to predict infarct size after coronary reperfusion; it is recommended as routine measurement in patients undergoing chemotherapy; it has been proposed as predictor of risk of ventricular arrhythmias; it may be applied to guide placement of the pacing lead in patients receiving cardiac resynchronization therapy amongst others [1]. Strain is more sensitive than ejection fraction as a measure of systolic function [1] and has better prognostic value [2].

Yet, the compelling added diagnostic value is tempered by a major clinical concern connected to the reported poor reproducibilty between the solutions provided by different vendors [3]. Such disagreement is not only due to obvious differences in accuracy coming from different technical implementations, but also to a lack of consensus on the definitions of the quantities of interest: Lagrangian vs. Eulerian strain; endocardial vs. mid-wall; end-systolic vs. peak systolic; definition of average values; definitions of the segments; etc. Unfortunately, these sources of inconsistency are not easily accessible since the underlying technical choices are not disclosed. Overall, this still holds back a more widespread dissemination of the STE technology. To address this issue, the European Association of Cardiovascular Imaging (EACVI), the American Society of Echocardiography (ASE) along with representatives from all vendors have been endorsing a concerted effort (a "task force") aimed at reducing intervendor variability of strain measurements [4].

Importantly, part of this effort has resulted in a first consensus document providing definitions and procedures to compute global and segmental longitudinal strain [5]. A further activity consisted in the quantification of inter-vendor differences through head-to-head comparison studies both *in-vivo* [6] and *in-silico* [7]. Unlike an *in-vivo* setup, an *in-silico* evaluation makes it possible to assess the absolute accuracy of a method in a fully controllable and reproducible setting [7]. In a first study, a synthetic dataset was therefore used to benchmark global longitudinal strain (GLS) measurements of nine different vendors of STE packages [7].

Synthetic sequences used in [7] were based on a kinematic model of cardiac contraction while a binary rule was used to assign ultrasound speckle texture, i.e. bright speckle inside

The work of Martino Alessandrini is funded by the European Union's Horizon 2020 research and innovation programme under the Marie Sklodowska-Curie grant agreement No 659082.

Asterisk denotes corresponding author. M. Alessandrini is with the Department of Electrical, Electronic and Information Engineering, University of Bologna, viale Risorgimento 2, 40127, Bologna, Italy and was with the Laboratory on Cardiovascular Imaging and Dynamics, University of Leuven, 3000 Leuven, Belgium when the study was designed. Email: martino.alessandrini@gmail.com

B. Chakraborty, B. Heyde and J. D'hooge are with the Laboratory on Cardiovascular Imaging and Dynamics, University of Leuven, 3000 Leuven, Belgium.

M. De Craene are with Philips Research, Medisys, 92156 Suresnes, France.

O. Bernard is with Universit de Lyon; CREATIS; CNRS UMR5220; Inserm U1044; INSA-Lyon; Universit Lyon 1; 69622 Lyon, France.

M. Sermesant is with the Inria-Asclepios Project, BP 93 06902 Sophia Antipolis, France.

This article has been accepted for publication in a future issue of this journal, but has not been fully edited. Content may change prior to final publication. Citation information: DOI 10.1109/TUFFC.2017.2786300, IEEE Transactions on Ultrasonics, Ferroelectrics, and Frequency Control

the myocardium and darker speckle elsewhere. The parametric motion model allowed modifying global motion descriptors and therefore to evaluate GLS sensitivity while the relative contrast between myocardium and surrounding regions could be adjusted to measure robustness to noise [7].

Despite the important insights provided by [7], such a simple simulation setup faced intrinsic limitations. On the one side, the simple speckle model could over-simplify, and therefore bias, the tracking problem. On the other, the global motion model could not be used to alter, and therefore benchmark, regional function [7]. There is thus a compelling need for more representative ground truth data for STE algorithms.

Recently, we have described a pipeline to simulate realistic ground truth sequences for 3D STE algorithms [8]. The pipeline used a complex electro-mechanical heart model to compute realistic physiological and pathological motion patterns which could account for regional dysfunction [9]. Moreover, the simulated 3D sequences were visually similar to real recordings thanks to a strategy that allowed sampling the synthetic speckle texture from a real volumetric recording. The pipeline in [8] was recently used to benchmark several 3D speckle tracking algorithms from academia [10]. Recently, that framework was extended to the simulation of, cine and tagged, magnetic resonance (MR) datasets [11].

Yet, 3D echocardiography is still an emerging technology in the clinic and therefore the priority, as embodied by the EACVI/ASE/Industry task force, is so far directed to 2D echocardiography only [5], [7]. Unfortunately, the pipeline in [8] cannot be used directly to simulate reliable 2D ground truth sequences. Indeed, simple slicing of the simulated 3D volumes obtained with [8] would not produce representative 2D simulations since i) the field of view in 2D is typically wider, ii) the image quality (i.e. spatial resolution) is typically higher. Therefore, we describe here a new framework to simulate representative 2D ground truth synthetic sequences for 2D STE algorithms.

As in [8], [10], the ultrasound images are simulated from a cloud of point scatterers. To have realistic speckle texture, scattering amplitude is sampled from a real clinical recording working as a ”template”. An electromechanical (E/M) cardiac model is then used to displace the scatterers inside the myocardium and therefore to have a realistic heart motion in the simulated image sequences. Yet, unlike in [8], in order to obtain realistic 2D simulated images we employ 2D clinical recordings as templates. This implies solving the consequent 2D/3D spatio-temporal registration problem between the 2D template and the 3D ground truth motion given by the electro-mechanical model instead of a 3D/3D registration problem as in [8]. Further, we include a strategy to mitigate the existing border artifacts visible in [8] at the interface between the myocardium and the blood pool. These are dealt with by implementing a smooth transition between the speckle properties in the two regions. Of note, such border artifacts were often identified as a source of poor realism in [8]. In addition, most importantly in our context, border artifacts could bias the initial segmentation step of a STE algorithm. Finally, unlike [8], the new 2D pipeline sets a prescribed density of incoherent scatterers in the myocardium. This overcomes a further limitation of [8], where speckle coherency was found to be unrealistically high. High temporal coherency could also bias the tracking problem. As in [8], the ultrasound images were simulated from the scatter maps by using the fast ultrasound simulator named “COLE” [12].

By changing the ground truth motion model, the adopted template recording and the probe settings in the ultrasound simulator, the new pipeline is used to generate a diverse set of 105 ground truth sequences encompassing i) healthy and ischemic motion patterns, ii) most common apical probe orientations (i.e. 2 chamber, 3 chamber and 4 chamber) iii) and vendor-specific image quality from seven systems. This last aspect in particular was the result of a concerted effort together with some representatives from the vendors involved who engaged to provide high quality template sequences for our study and to disclose some details of the acquisition setup to be used in the ultrasound simulator [12]. The dataset can therefore be used to benchmark sensitivity to changing global and regional function as well as changing image appearance between vendors. This dataset is made available to the research community at our project web-page (cf. Sect. IV-A).

A preliminary version of this study was presented in the proceeding paper [13], which is extended in several ways. At first, the database presented here is larger (105 sequences vs. 4 in [13]) and more diverse in terms of probe orientation (2, 3 and 4 chamber views vs. 2 and 4 chamber in [13]) and motion pattern (5 kinds of ischemia vs. 2 in [13]). Moreover, unlike [13], we include vendor specific speckle texture from seven different vendors. Finally, none of the techniques presented here to solve the simulation artefacts were present in [13]. Additionally, we show the feasibility of the provided synthetic dataset by using it in the evaluation of one technique developed recently in our group [14].

The paper proceeds as follows. In Sect. II, we describe the simulation pipeline. In Sect. III we define the ground truth quantities derived from the synthetic data and present the evaluation of the considered ST technique. Sect. IV describes the simulated dataset and the evaluation result. Sect. V follows with the discussion while the paper is concluded in Sect. VI.

II. Simulation Pipeline

The flowchart of the proposed simulation pipeline is provided in Fig. 1. Each block contains a reference to the Section in the paper where its content is described. Real ultrasound recordings are used to transfer realistic texture to the simulated sequences (block 1). The first step in the simulation pipeline is to align a detailed bi-ventricular 3D anatomy (block 2) to the 2D template recording. The result is displayed in block 3. The electro-mechanical simulator is run on the 3D anatomy to generate the ground truth motion field for one cardiac cycle (block 4). In order to apply the ground truth motion field to the 2D template, the cardiac motion in the template recording has to be computed (block 5) and compensated for (block 6). The ground truth motion is then used to displace a cloud of point scatterers (block 7). Thanks to the composition between the ground truth and the computed motion field, scattering amplitude can be sampled from the template recording. The

This article has been accepted for publication in a future issue of this journal, but has not been fully edited. Content may change prior to final publication. Citation information: DOI 10.1109/TUFFC.2017.2786300, IEEE Transactions on Ultrasonics, Ferroelectrics, and Frequency Control

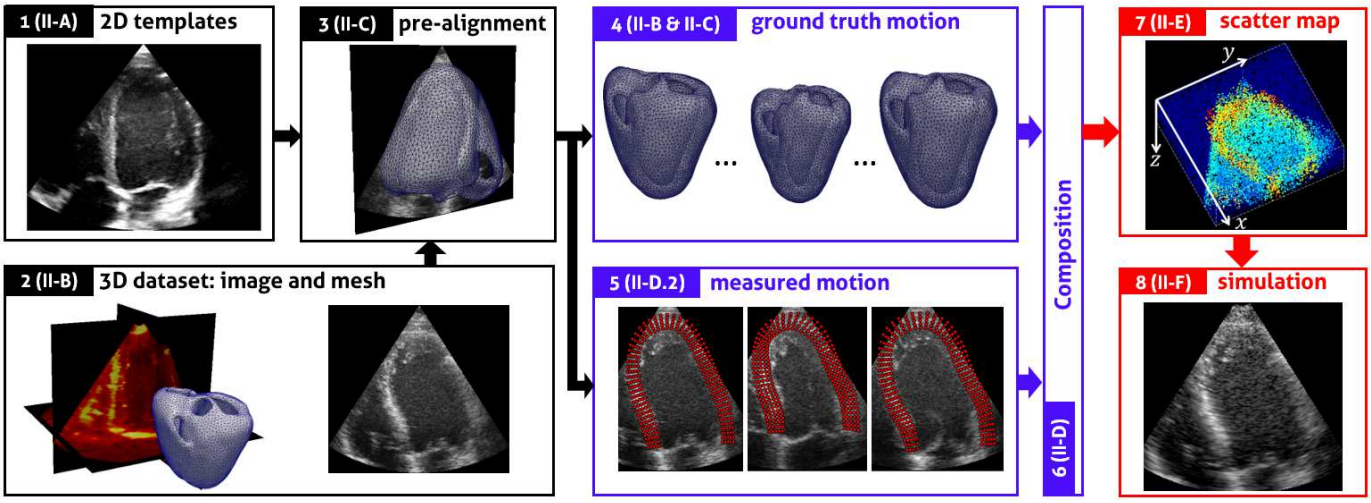

Fig. 1. Flowchart of the proposed simulation pipeline. Each block reports between brackets the Section describing its content. The black part contains the necessary pre-processing to align the 2D template with the 3D mesh. The blue part contains the computation of the synthetic displacement field (*i.e.* the ground truth). The red part contains the ultrasound simulation. Please refer to the main text for a detailed description.

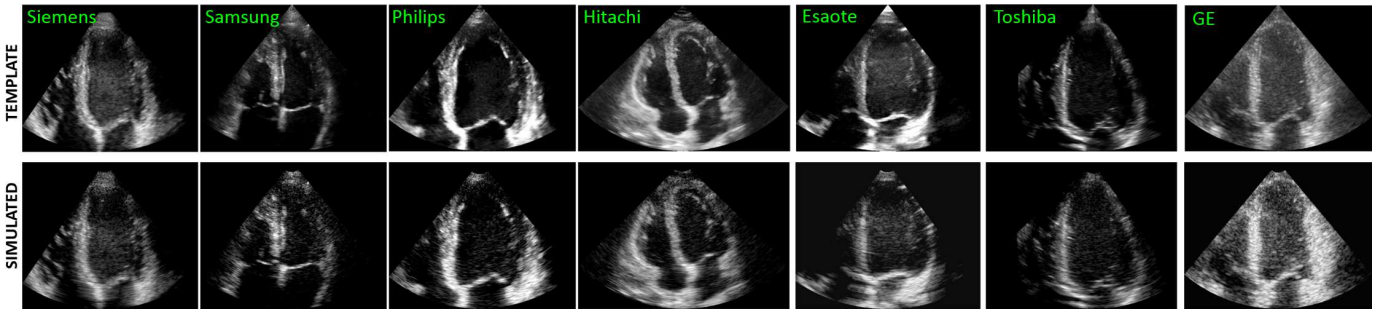

Fig. 2. Sample template sequences (4-ch, end diastolic frame) from the 7 vendors (first row) and corresponding simulated images (second row).

ultrasound simulator is then run on the scatter map to generate the synthetic images (block 8). The simulated sequence will look like the template recording but cardiac motion will be fully determined by the electro-mechanical simulation and, hence, available for benchmarking. A detailed description of the pipeline follows.

A. Template recordings

For each vendor involved, we used one apical 4 chamber (4-ch), one apical 3 chamber (3-ch) and one apical 2 chamber (2-ch) cine recording as template for the subsequent simulation steps. One full cardiac cycle from end-of-diastole (ED) was retained from each recording. We included the 7 manufacturers of ultrasound systems already involved in the EACVI/ASE/Industry standardization task force [6], [7]. The specific vendors and relative systems were therefore: General Electrics, GE (Vivid E9 version 112.1.3); Hitachi-Aloka (Prosound α7 CV version 6.1); Esaote (MyLab Alpha); Philips (iE 33 Vision 2012); Samsung (EK07); Siemens (SC2000 version 3.5) and Toshiba (Artida version 3.0).

The template recordings were retrieved from the database created in the context of the first inter-vendor study [6] and available at the University Hospital Gasthuisberg, KU Leuven, Leuven, Belgium. In this version of the dataset we were interested in generating, for each vendor, synthetic recordings with good visual quality. As explained later, this implies working with high quality templates. Hereto, the selected sequences were then transmitted to the representatives of the relevant vendors for quality check. Whenever considered necessary, alternative, good quality, sequences were sent back to us by the vendors. As such, 21 (7 vendors $\times$ 3 apical views) multi-vendor high quality template recordings were available. Example frames are provided in Fig. 2, first row. For all vendors but GE, templates were provided as dicom data exported from the respective systems, from which the image sector was extracted by using custom software written in MATLAB R2017a (The MathWorks, Inc., Natick, Massachusetts, United States). GE provided instead raw radiofrequency (RF) signals along with the MATLAB scripts to reconstruct the images.

Additionally, all vendors agreed to disclose some of the acquisition settings, such as temporal resolution, scan depth, focus depth, beam density, center frequency, bandwidth. These settings were used to make the simulated acquisition sequence as close as possible to the real systems, see Sect. II-F.

B. 3D geometry and electromechanical model

The E/M simulations used were the same as in [8]. Briefly, left and right ventricles were segmented from a 3D ultrasound recording (Philips iE33 ultrasound machine with a X5 matrix array transducer) by using proprietary model-based full

This article has been accepted for publication in a future issue of this journal, but has not been fully edited. Content may change prior to final publication. Citation information: DOI 10.1109/TUFFC.2017.2786300, IEEE Transactions on Ultrasonics, Ferroelectrics, and Frequency Control

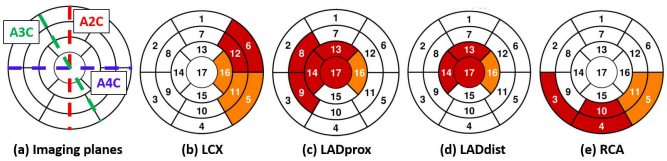

Fig. 3. Bull's eye plots with imaging planes (a) and an illustration of ischemic (red) and neighboring (orange) segments for the LCX (b), LADprox (c), LADdist (d), and RCA (e) mechanical simulations.

heart segmentation software by Philips (cf. Fig. 4(a)). The segmented volume was then converted into a tetrahedral mesh by using a MATLAB wrap of the Computational Geometry Algorithms Library (CGAL)[1] [15]. The segmented geometry was then animated by applying the Bestel-Clement-Sorine (BCS) E/M model [16] as implemented in the Simulation Open Framework Architecture (SOFA) framework[2] [17] developed by Inria, CNRS, USTL, UJF, MGH. By altering the model's contractility and stiffness we simulated three kinds of segments: normal, mildly-ischemic and fully-ischemic. Segments were defined as per the standard 17 segments model defined by the American Heart Association (AHA) [18]. The three kinds of segments were combined to realize 5 motion patterns, one healthy and four ischemic ones corresponding to: a distal and proximal occlusion of the Left Anterior Descending artery (LADdist and LADprox respectively); occlusions of Right Coronary Artery (RCA) and Left Circumflex (LCX). Please refer to [8] for more details.

As such, a series of tetrahedral meshes was available for each simulation to span one cardiac cycle starting from end-of-diastole. Temporal resolution (i.e. the number of meshes), was adjusted for each vendor in order to match the frame rate of the specific system. Fig. 3 illustrates the 3 considered image planes and the mechanical properties of each segment in the four ischemic simulations. Of note, the right ventricle was only used to have a balanced E/M simulation. Our focus being on left ventricular dynamics, the right ventricle (RV) was therefore excluded from the meshes resulting from the E/M simulation. Hence, in the following, when referring to the 3D model we will be referring to the left ventricle (LV) only.

C. Initial alignment of the 3D simulation and the 2D template

The first step was to align, for each vendor and each apical view, the 3D simulation and the 2D template at time 0, i.e. at end-of-diastole. As mentioned, the 3D geometry was obtained by segmenting a 3D echocardiographic scan. The procedure consisted of the following steps, as illustrated in Fig. 4:

- From the 3D echocardiographic scan used to construct the 3D geometry we extracted one 2D slice corresponding to the specific apical view of the 2D template. Hereto, we used a slicing plane containing the LV long axis and rotated of 0, 60 or 90 degrees depending on whether the 2D template corresponded to a 4-ch, 3-ch or 2-ch view, respectively. Angles are referred to a clockwise rotation looking from the LV apex to the LV base. The segmentation of the 3 extracted apical slices was directly available from the 3D model, cf. Fig. 4(b) for the extracted 4-ch slice;
- The LV myocardium was contoured manually on the first frame of the 2D template. This contour was used to drive the alignment with the 3D model, as described later. In order for this alignment to be correct, it was

[1] http://www.cgal.org/
[2] https://www.sofa-framework.org/

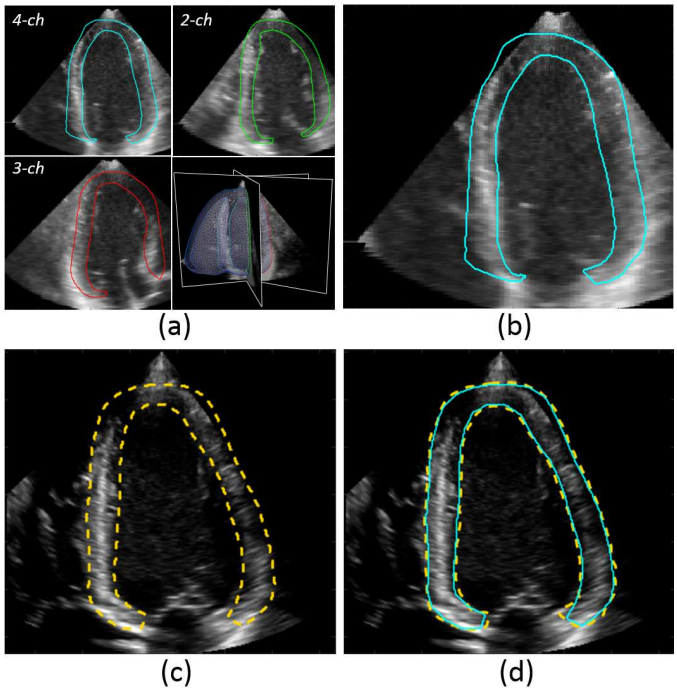

Fig. 4. The 3 apical views are sliced from both the 3D image volume and the 3D mesh by using fixed rotation angles around the LV long axis, as described in the text. Panel (a) illustrates the 3 extracted image slices, the full 3D anatomical model (i.e., the transparent tetrahedral mesh overlaid) as well as the intersections of the 3D model with the sliced image planes: in cyan, the intersection with the 4-ch slice; in green, the intersection with the 2-ch slice; in red, the intersection with the 3-ch slice. Panel (b) illustrates the 4-ch slice along with the associated contour (in cyan). Panel (c) illustrates the first frame of the 4-ch template recording from Toshiba along with the associated segmentation (the dashed orange contour), drawn manually in order to match the cyan contour in (b). (d) The 3D geometry is deformed in order to match the template frame. The final deformation aligns the green contour onto the orange one.

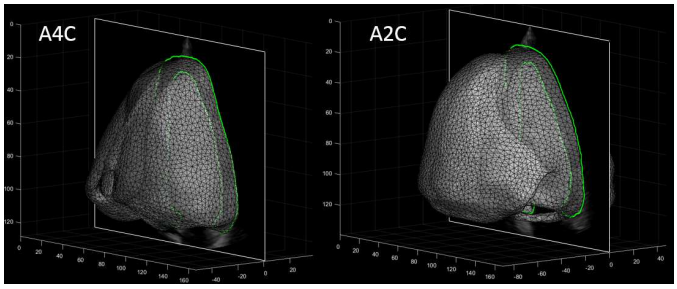

Fig. 5. Result of the 3D/2D registration step described in Sect. II-C. After registration, the 3D bi-ventricular model (i.e., the tetrahedral mesh in the figure) is aligned with the first frame of the 2D template recording. The green contour represents the intersection between the 3D model and the image plane. The result of the alignment is illustrated for an apical 4-ch (left) and an apical 2-ch (right) view from Toshiba.

This article has been accepted for publication in a future issue of this journal, but has not been fully edited. Content may change prior to final publication. Citation information: DOI 10.1109/TUFFC.2017.2786300, IEEE Transactions on Ultrasonics, Ferroelectrics, and Frequency Control

essential to have consistent contouring between the 2D template and the sliced 3D volume. In practice, this implied having a consistent definition of the cut levels at the LV base. To ensure consistency, the 2D template was segmented by using the corresponding segmentation of the sliced 3D volume as a visual reference. This process is illustrated in Fig. 4(c) for the 4-ch view from Toshiba: the LV myocardium was contoured manually (dashed orange contour) on the template by using the cyan contour in Fig. 4(b) as a visual reference.

- The segmentation of the sliced 3D geometry (cyan contour in Fig. 4(b)) was then registered onto the segmentation of the 2D template (dashed orange contour in Fig. 4(c)). Hereto, both contours were initially converted to binary masks and aligned by rigid registration. To refine the alignment, we used non-rigid free-form registration as implemented in the Medical Image Registration Toolbox, developed by Andriy Myronenko and available open source at[3]. Sum of squared differences was used as a dissimilarity metric and its computation was restricted in space to a mask surrounding the myocardium. The deformation field was parameterized with B-splines and regularization was enforced by Laplacian penalization of the displacements of the B-spline control points [19]. The parameters of the registration algorithm (i.e. grid spacing, number of pyramidal levels and regularization weight) where tuned by optimizing visual matching. The final alignment of the two contours is illustrated in Fig. 4(d);
- The transformation between slices, as computed in the previous step, was used to align the first of the 3D geometries. Hereto, the 2D transform, defined on the image plane, was used to displace the in-plane coordinates of the nodes of the 3D mesh. As mentioned, this involved an initial rigid registration followed by a non rigid refinement. To keep the 3D deformed geometry balanced, the out of plane coordinate of the mesh nodes was scaled by using the same scaling factor found in the initial rigid registration step. This way, a possible change in size was distributed uniformly along the 3 dimensions. At the end of this step, the 2D template and the 3D geometry were aligned, as illustrated in Fig. 5 for the Toshiba template.
- The same transform found for the first 3D geometry was then applied to the full time series.

As such, for each vendor and each apical view, we obtained a specific set of tetrahedral meshes corresponding to one simulated heart beat and initially (i.e. at time 0) aligned with the 2D image template. These meshes will define the ground truth values of deformation and strain for the specific template, as explained later in the manuscript. The following sections will explain how to compute a spatio-temporal transform that extends the alignment between the 2D template and the 3D simulation to the full cardiac cycle. Such a transform will be fundamental to sample scatter amplitude from the template recording and therefore to obtain realistic simulated images. In the following, we will assume therefore that the 3D geometries have been pre-aligned as described in this section.

[3]https://sites.google.com/site/myronenko/research/mirt

D. Spatio-Temporal Alignment

1) Template space and simulation space: Template and simulation have different dimensionality. The template is defined on the image slice. A point in the template space is therefore $\mathbf{y} = [y_1, y_2] \in \Omega_{im}$, with $\Omega_{im} = w \times h$, being w and h image width and height. The simulation has an additional dimension perpendicular to the image plane. A point in the simulation space is therefore $\mathbf{x} = [x_1, x_2, x_3] \in \Omega_{sim}$, with $\Omega_{sim} = \Omega_{im} \times I_d$, being I_d a 1D segment of length d centered on the image plane and perpendicular to it. This is also illustrated in Fig. 5 and Fig. 6. The thickness d of the 3D slab was chosen empirically to prevent out of plane motion components in the E/M model from creating holes in the simulated images.

2) Motion field in the template: The goal is to find a displacement field in the template recording. Hereto, we used an elastic registration technique [14] to compute a set of temporally corresponding points sampling the myocardium uniformly over time. Thin plane splines (TPS) [20] were then used to extrapolate cardiac motion from the discrete point set to the entire image space.

More formally, given the initial position of a point $\mathbf{y}$ at time 0, TPS find its matched position $\mathcal{F}(\mathbf{y}, t) = \mathbf{y} + \mathbf{f}(\mathbf{y}, t)$ at time t, being $\mathbf{f}(\cdot, t)$ the extrapolated displacement field at time t.

3) Extrapolating the synthetic cardiac motion: In a similar manner, we used TPS to extrapolate cardiac motion to surrounding regions in the simulation space by using the nodes of the E/M meshes as control points. Specifically, given a point $\mathbf{x}$ at time 0, its position at time t is $\mathcal{G}(\mathbf{x}, t) = \mathbf{x} + \mathbf{g}(\mathbf{x}, t)$, being $\mathbf{g}(\cdot, t)$ the extrapolated displacement field at time t.

4) Temporal matching: The goal is to synchronize template and simulation by aligning corresponding phases of the cardiac cycle. Namely, we seek for a mapping $t_T = t_T(t_S)$ between the time axis in the simulation (t_S) and the template recording (t_T). As in [8], we linearly stretch/compress the t_T axis in order to match a set of relevant cardiac events. Hereto, we used three cardiac events for matching: first end-of-diastole (i.e. the first frame), end-of-systole (ES) and the second end-of-diastole (i.e. the last frame). End of systole was identified visually on template and the simulation based on minimum volume of the LV chamber.

E. Scatter map generation

Each image frame was simulated from the combination of two scatter maps: one *coherent* scatter map and one *incoherent* scatter map. Both scatter maps evolved in time to account for cardiac motion. In both cases, scatterers were distributed on Ω_{sim} by following a uniform random distribution. The total number of scatterers N_s was established experimentally in order to have realistic speckle statistics in the simulated images. This evaluation is presented in [8]. In total, we used 2 million scatterers for each scatter map.

This article has been accepted for publication in a future issue of this journal, but has not been fully edited. Content may change prior to final publication. Citation information: DOI 10.1109/TUFFC.2017.2786300, IEEE Transactions on Ultrasonics, Ferroelectrics, and Frequency Control

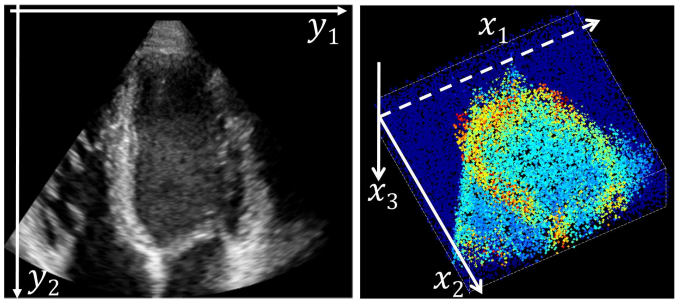

Fig. 6. The first frame of the 2D template recording is illustrated in the left panel. y_1 and y_2 represent the coordinate axes in the image space. The scatter map corresponding to the first simulated frame is illustrated in the right panel. Color encodes scatter amplitude according to a "jet" color-map: blue means low amplitude and red means high amplitude. Scatter amplitude was sampled from the template frame in the left panel. x_1, x_2 and x_3 are the coordinate axes in simulation space. The through-plane coordinate x_3 was added to avoid the effect of out-of-plane motion components, as discussed in the main text.

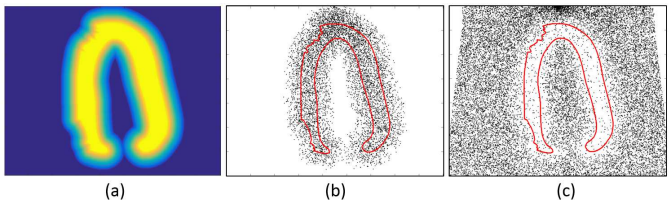

Fig. 7. (a) Probability map used to mix coherent and incoherent scatter maps. (b) Selected coherent scatterers. (c) Selected incoherent scatterers. The red contour in (b) and (c) denotes the myocardial mask. Note that we allow both incoherent scatterers inside the myocardium and coherent scatterers in the background. The scatter map was sub-sampled for readability of the figure.

1) Scatter map on the first frame: We generated N_s scatterers randomly in Ω_{sim}. The position of the i-th scatterer is denoted as $\mathbf{x}_i = [x_1^i, x_2^i, x_3^i]$, with $i = 0, \cdots, N_s - 1$. The x_1 and x_2 coordinates belong to the image plane while x_3 is the out of plane coordinate (i.e. the azimuth), as illustrated in Fig. 6.

2) Coherent scatter map: The coherent scatter map was computed by taking the scatterers generated on the first frame and propagating them over time by using $\mathbf{x}_i(t_S) = \mathcal{G}(\mathbf{x}_i(0), t_S)$. Temporal coherency is given by the fact that the same scatterer is followed over the full simulation.

3) Incoherent scatter map: At each simulation time t_S, we regenerated new random scatterers in the ED frame and moved them to their correct configuration by $\mathbf{x}_i(t_S) = \mathcal{G}(\mathbf{x}_i, t_S)$. Therefore, unlike the coherent scatter map, there was no correspondence between scatterers at different simulation times in the incoherent scatter map.

4) Final scatter map: The final scatter map was obtained by mixing, at each simulation time, the coherent and incoherent scatter maps. Conceptually, coherent scatterers were mainly placed in the myocardium to enable speckle tracking, while incoherent scatterers were mainly placed in the background to account for the typical lack of speckle coherency in the blood. In our previous work [8], [13], the assignment was made based on a binary rule: coherent scatterers only in the myocardium and incoherent scatterers only in the background. This abrupt transition was sometimes the origin of mild artifacts at the interface between the two regions. To remove this effect, we applied here a smoother transition. This was implemented by using a smooth mask, as illustrated in Fig. 7(a), which, for each position, defines the probability of accepting a coherent scatterer and rejecting an incoherent one. The probability map was obtained by decreasing linearly from a value $p = 0.9$ inside the myocardium to a value $p = 0$, with a transition zone of 15 mm. The width of the transition zone was tuned visually in order maximize the realism of the simulations. Of note, we allowed a 10% of incoherent component inside the myocardium. The presence of incoherent speckle inside the myocardium is observed experimentally.

To apply the acceptance/rejection rule, we assigned each scatterer a number w_i, picked randomly in the interval $[0, 1]$. Therefore, we accepted a coherent scatterer $\mathbf{x}_i$ if $w_i < p(\mathbf{x}_i)$, otherwise we rejected it. Similarly, we accepted an incoherent scatter if $w_i > p(\mathbf{x}_i)$. The set of selected coherent and incoherent scatterers is illustrated in Fig. 7.

Of note, this is different from what done in [11], where a smoothing mask was used to weight scattering amplitude between myocardium and surrounding structures. By that, speckle coherency in the myocardium was expected to remain high as in [8]. High speckle coherency was identified as a source of poor realism in [8] and could over-simplify the speckle tracking problem.

5) Scattering amplitude: The amplitude a_i of myocardial scatterers (i.e. belonging to the region enclosed by the E/M meshes) was sampled from the first frame of the template recording and kept constant over time, i.e. $a_i(t_S) = a_i(0) = I(\mathbf{y}_i, 0)$, where $\mathbf{y}_i = [x_1^i, x_2^i]$ and $I(\cdot, k)$ denotes the $k-th$ template frame. This choice was made to enforce speckle coherency inside the myocardium. The amplitude of background scatterers was instead sampled from the matched frame in the template recording, i.e. $a_i(t_S) = I(\mathcal{F}(\mathbf{y}_i, t_T), t_T)$. This strategy allowed having realistic moving texture for surrounding structures. Moreover, as in [8], to compensate for the logarithmic compression performed by ultrasound systems before display, we applied a mapping $\hat{a}_i = F(a_i)$ such that $20 \log_{10}[F(a_i)] + dB = dB \cdot (a_i/255)$, where dB is the desired contrast in decibel in the simulated image. We have assumed a common 8 bit representation for template recordings.

F. Ultrasound simulation

The ultrasound simulations were performed with the in-house COLE simulator [12]. We used the 3D scatter maps to simulate 2D images corresponding to azimuth $x_3 = 0$. Synthetic probe settings (scan depth, focus depth, field of view, beam density, center frequency, sampling frequency, bandwidth) were specialized by using the values communicated by each vendor upon signature of non disclosure agreements. Simulated RF lines were envelope detected, log compressed and scan converted to obtain B-mode voxel images. Scan converted images were re-sampled to match the pixel size of the corresponding template. Image reconstruction was therefore performed using our in-house algorithms which may differ from the company reconstruction algorithms. This in itself could have impact on the appearance of the resulting images (cf. Fig. 2).

This article has been accepted for publication in a future issue of this journal, but has not been fully edited. Content may change prior to final publication. Citation information: DOI 10.1109/TUFFC.2017.2786300, IEEE Transactions on Ultrasonics, Ferroelectrics, and Frequency Control

As such, we generated a dataset of 105 ground truth sequences (7 vendors $\times$ 3 apical views $\times$ 5 motion patterns.).

III. Evaluation

A. Ground truth

We defined ground truth displacement and strain in agreement with the recent recommendations from the EACVI/ASE/Industry task force [5]. Hereto, we defined a set of seed points sampling the LV myocardium regularly along the longitudinal (36 points) and radial (5 points) directions. Longitudinal sampling was parameterized by the arc-length as computed with spline interpolation. The radial direction was computed as being normal to the longitudinal one. The 5 radial points were distributed uniformly between endocardium and epicardium. Endocardial and epicardial masks were defined manually on the first frame of each simulated recording. Points were further subdivided in 6 segments (in clockwise order: left-base, left-middle, left-apical, right-apical, right-middle, right basal), obtained by splitting the endocardial contour into 6 parts with the same arc-length.

The seed points were anchored to the E/M by keeping barycentric coordinates constant over time. To account for the fact that the E/M model might produce out-of-plane motion components we constantly re-project the seed point on the image plane at each frame. As such, a 2D cloud of corresponding points was available for the full simulated cine-loop. We call these points $\mathbf{p}^i_{k_l,k_r}$, where $k_l = 0, \cdots, N_l - 1$ indicates the longitudinal coordinate, $k_r = 0, \cdots, N_r - 1$ indicates the radial coordinate and $i = 0, \cdots, N_{sim} - 1$ is the time frame. $N_l = 36$ is the number of longitudinal points, $N_r = 5$ is the number of radial points and N_{sim} is the (vendor dependent) number of simulated frames.

The time series of seed points were used to define the ground truth strain values. By using Lagrangian formulation [5], longitudinal (L-) strain at simulation time i was computed as $\epsilon^i_L = (L^i - L^0)/L^0$, where L^i is either the length of a segment (segmental strain) or the length of the LV contour (global longitudinal strain, GLS). Arc-length was computed by using a continuous interpolation by cubic splines. Namely, cubic spline interpolation was used to obtain a parametric function $\mathbf{p}^i_{k_r}(l)$ in the continuous longitudinal variable $l \in [0, L^i_{k_r}]$, being $L^i_{k_r}$ the length of the full arc at transmural layer k_r measured by accumulating euclidean distances, i.e. $L^i_{k_r} = \sum_{k_l=0}^{N_l-2} \|\mathbf{p}^i_{k_l+1,k_r} - \mathbf{p}^i_{k_l,k_r}\|$. Arc-length was then computed by numerical integration:

$$L(l_a, l_b)^i = \int_{l_a}^{l_b} \left\| \frac{d\mathbf{p}^i_{k_r}(l)}{dl} \right\| dl. \tag{1}$$

Segmental and global strain were computed by setting the integration interval appropriately (for longitudinal strain, $l_a = 0$ and $l_b = L^i_{k_r}$). L-strain could be evaluated at 5 transmural layers. Radial (R-) strain was defined similarly by considering the relative change in distance between points in the radial direction. Segmental and global (GRS) R-strain were computed by averaging local estimates. Strain drift was compensated for retrospectively by distributing it linearly over the full cardiac cycle.

B. Considered Speckle Tracking Algorithm

To illustrate that the generated sequences are suited for ST we used them to evaluate one recent ST technique developed in our lab [21]. The technique is based on elastic registration and uses a B-splice parametrization of the displacement field. The displacement is retrieved by minimizing an energy function expressed as the sum of a data term and a penalty. Sum-of-squared-differences (SSD) between the intensity of the two registered frames was used as a data term and bending energy was used as a penalty.

The algorithm returned a dense displacement field $\mathbf{d}_{i\to i+1}(\mathbf{x})$ between pairs of subsequent frames $I_i(\mathbf{x})$ and $I_{i+1}(\mathbf{x})$. The computed displacement field was used to propagate the ground-truth seed points $\mathbf{p}^0_{k_l,k_r}$ available on the first frame through the entire cardiac cycle. Namely, a new set of points $\tilde{\mathbf{p}}^i_{k_l,k_r}$ was incrementally computed as $\tilde{\mathbf{p}}^i_{k_l,k_r} = \tilde{\mathbf{p}}^{i-1}_{k_l,k_r} + \mathbf{d}_{i-1\to i}(\tilde{\mathbf{p}}^{i-1}_{k_l,k_r})$ for $i = 1, \cdots, N_{sim-1}$ and $\tilde{\mathbf{p}}^0_{k_l,k_r} = \mathbf{p}^0_{k_l,k_r}$ for $i = 0$. As such, for each simulated sequence we had the trajectory estimated by the speckle tracking algorithm $\tilde{\mathbf{p}}$ and the real trajectory $\mathbf{p}$ given by the ground truth. Tracking accuracy was then measured by comparing the two. The computed set of points $\tilde{\mathbf{p}}$ were used to compute segmental and global strain as described above and compared against the ground truth. Hereto, the slope (α) of the regression line between the estimate and the ground truth, the regression coefficient (ρ), bias (μ) and limits of agreement (LOA = 1.96σ) were considered as performance indexes. Further, we tested the classification accuracy when using the computed strain values to detect ischemia by measuring the area under the curve (AUC) of the receiver operating characteristic (ROC) curves. The ROC curves were computed from a progressive threshold by assuming ES (absolute) strain values below the threshold as indicative of ischemia.

Fisher's transformation was used to test the hypothesis of no correlation. Strain bias was instead evaluated with a t-test. The statistical significance of the reported AUC values (i.e., of AUC> 0.5) was tested with the non-parametric technique described in [22].

The algorithm was tuned to maximize tracking accuracy on the healthy simulated GE sequences and tested on the remaining data. The most sensitive parameters in the evaluated algorithm were the weight put on the penalty term and the spacing between the B-spline knots. Both parameters impact the smoothness of the retrieved deformation field and the sensitivity to small deformations.

IV. Results

A. The open access database

Example images simulated with the proposed pipeline for the 7 vendors are given in Fig. 2. Please note the resemblance with the corresponding templates. Also, we stress that image reconstruction from the simulated RF signals was done with our in-house algorithm which may in general differ from the ones by the specific vendors. This might have an effect on the appearance of the simulated images.

This article has been accepted for publication in a future issue of this journal, but has not been fully edited. Content may change prior to final publication. Citation information: DOI 10.1109/TUFFC.2017.2786300, IEEE Transactions on Ultrasonics, Ferroelectrics, and Frequency Control

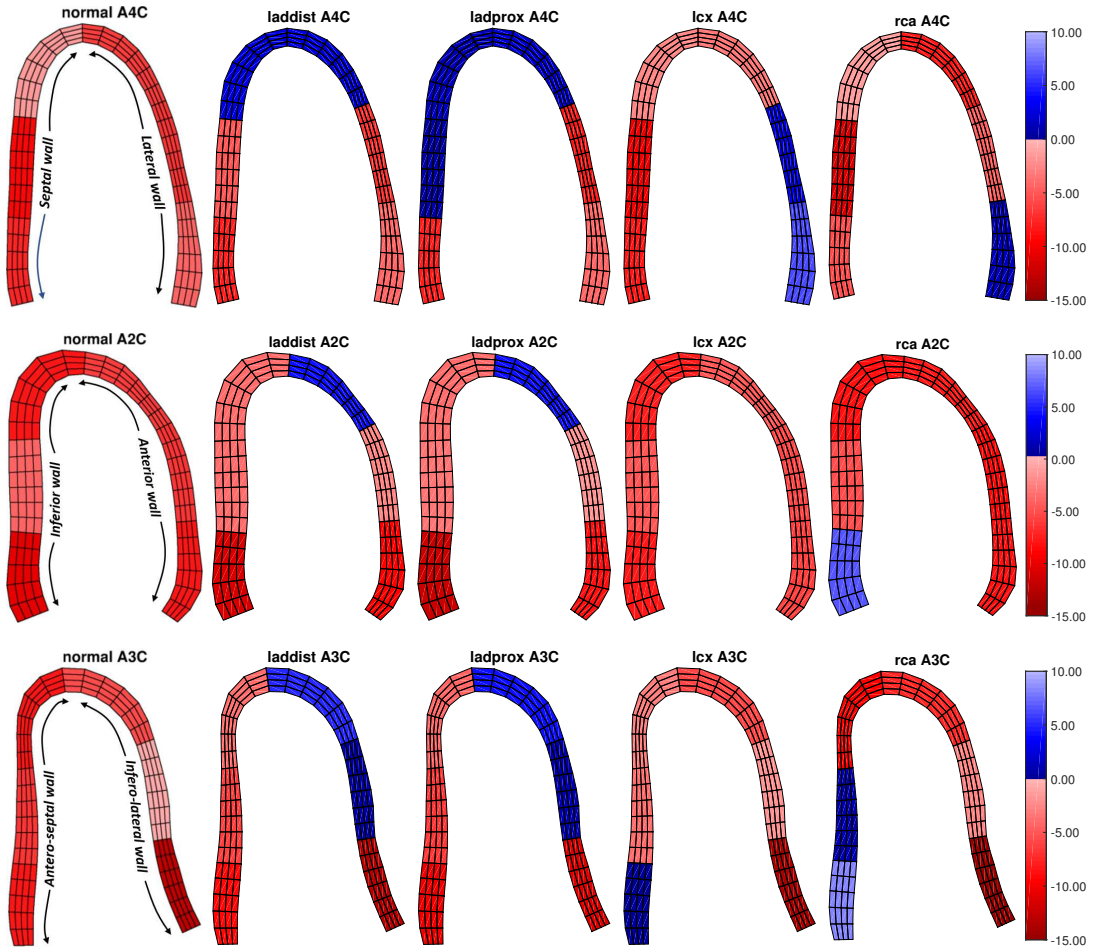

Fig. 8. Each image represents the LV myocardium in a 4-ch (top row), 2-ch (mid-row) and 3-ch (bottom row) view. The quadrangular meshes, represented as wire-frames, were obtained by taking the 36×5 ground-truth seed points as nodes. Columns correspond to different motion patterns (the healthy simulation in the first column and the 4 ischemic ones in the remaining columns). Segments are colored according to the average ground truth L-strain value over all vendors. Note that impaired segments are in agreement with cf. Fig. 3.

The open database of 105 sequences can be accessed either from our departmental web-page[4] or directly at http://bit.ly/SyntheticDataQA2DSTE. The database includes pixel images, the scatter maps, the ground truth seed points and the MATLAB scripts to compute ground truth values of global and segmental L- and R- strain. Simulated RF data cannot be distributed directly since they could enable reverse-engineering of the probe settings, which have been covered by non-disclosure agreements. Yet, synthetic RF data for arbitrary probe settings can be easily generated by a user from the provided scatter maps.

B. Mechanical properties of the synthetic dataset

Maps of segmental end systolic L-strain are presented in Fig. 8. Segments were colored according to the average values over all seven vendors, which were not necessarily equal due to the registration step in Sect. II-C. Note that impaired segments are in full agreement with Fig. 3. Simulated ischemia, therefore, effectively reduces regional LV function in the expected perfusion territories. Yet, values of L-strain for normal cases remain below the reported normality ranges. This point will be discussed further in the discussion section.

[4]https://gbiomed.kuleuven.be/english/research/50000635/50508167/open-data

C. Evaluation of the speckle tracking algorithm

The performance indexes for ES L-strain are reported in Table I. Strain accuracy varies between vendors due to the different image appearance. Fig. 9 displays the correlation plots for the seven vendors. Healthy and ischemic segments, defined according to Fig. 3, are colored in green and red, respectively. The separation between healthy and ischemic segments is also visualized by the Gaussian distributions on the x-axis for the ground truth and on the y-axis for the speckle tracking estimate. A measure of the superposition between the two classes is provided by the AUC in Table I. The AUC of the ground truth is reported in the last column of Table I.

The estimated segmental strain curves on the 4-ch LADdist simulated Toshiba sequence are displayed in Fig. 10. The estimated profiles follow closely the ground truth and dis-kinetic segments are recovered correctly on this sequence.

V. Discussion

We have presented a pipeline to generate realistic synthetic data for 2D speckle tracking algorithms. The pipeline was

This article has been accepted for publication in a future issue of this journal, but has not been fully edited. Content may change prior to final publication. Citation information: DOI 10.1109/TUFFC.2017.2786300, IEEE Transactions on Ultrasonics, Ferroelectrics, and Frequency Control

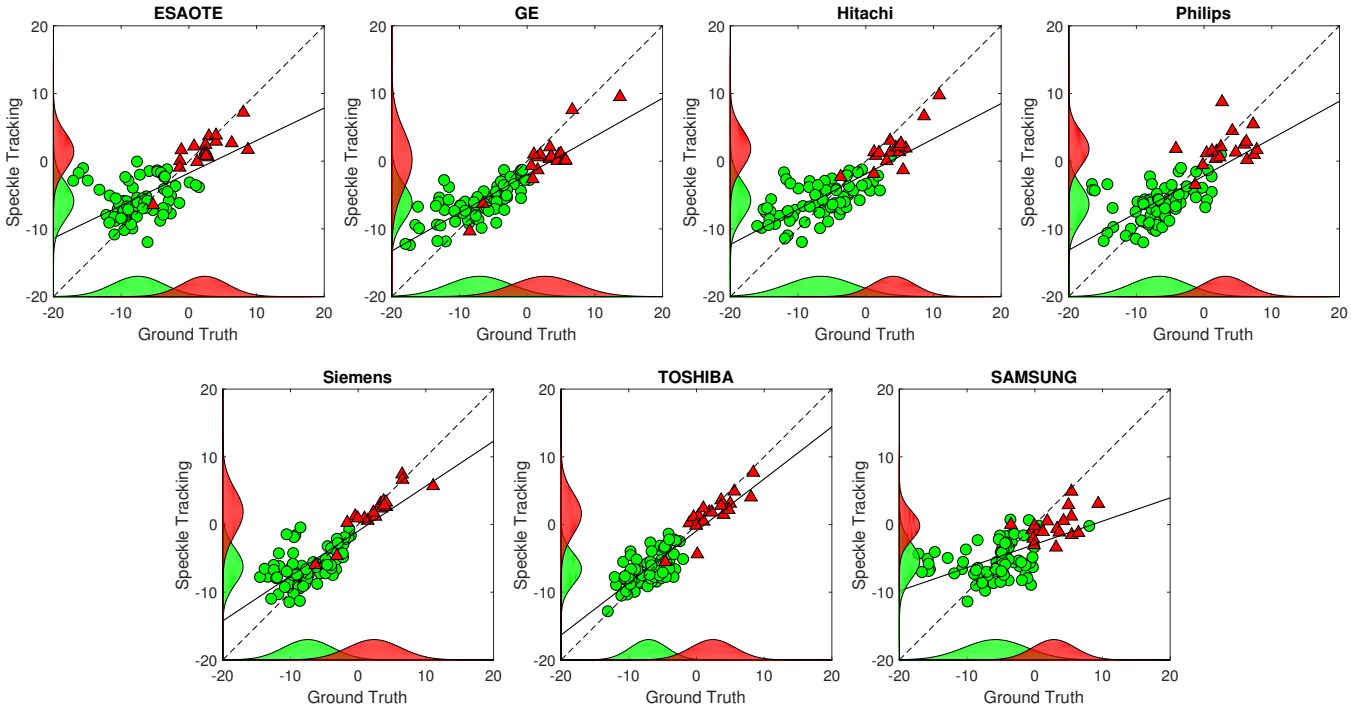

Fig. 9. Correlation plot between ground truth segmental L-strain (x-axis) and speckle tracking estimate (y-axis). Healthy segments are represented as green dots while ischemic segment as red triangles. The Gaussian distributions were computed from the sample mean and standard deviation and provide an intuition of the separation between classes.

TABLE I
RESULTS OF THE CONSIDERED IN-HOUSE SPECKLE TRACKING ALGORITHM, REPORTED SEPARATELY FOR EACH VENDOR SPECIFIC SYNTHETIC DATASET (FIRST COLUMN). SLOPE OF THE REGRESSION LINE (α), CORRELATION COEFFICIENT (ρ), BIAS (μ), LIMITS OF AGREEMENT (LOA) AND AREA UNDER THE ROC CURVE (AUC). ASTERISKS DENOTE STATISTICAL SIGNIFICANCE (REFER TO THE MAIN TEXT FOR ITS DEFINITION).

VENDOR	α	ρ	μ	LOA	AUC	AUC$_{GT}$
Hitachi	0.52	0.81*	0.30	7.59	0.99*	0.97*
Toshiba	0.77	0.89*	0.29	4.30	0.97*	0.99*
Esaote	0.48	0.60*	1.44	8.06	0.97*	0.98*
Samsung	0.33	0.56*	-0.60	8.87	0.94*	0.96*
Siemens	0.66	0.83*	0.89	5.87	0.96*	0.97*
Philips	0.55	0.73*	-0.02	7.60	0.99*	0.97*
GE	0.56	0.86*	0.29	6.59	0.91*	0.94*

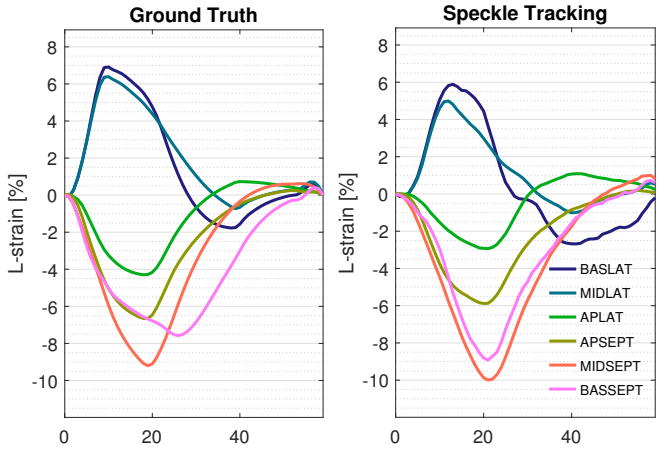

Fig. 10. Segmental L-strain on the synthetic 4-ch LCX Toshiba sequence: ground truth (a) and as estimated by the considered in-house speckle tracking algorithm (b).

used to generate an open access database of 105 synthetic sequences. The synthetic datasets are diverse in terms of motion pattern, probe orientation and speckle texture. In particular, we provide image qualities representative of 7 different ultrasound systems from different vendors. This was the result of a major logistic effort involving representatives from 7 major vendors of ultrasound systems who accepted to provide high quality template recordings and disclose some of the proprietary acquisition settings especially for this study. This dataset can therefore be used to measure sensitivity to changing global and regional function as well as changing image appearance between vendors.

In terms of mechanical properties, this dataset shares some of the limitations of the original pipeline for 3D simulations [8], [10]. Values of peak systolic longitudinal strain for the healthy case are below reported normality ranges [23]. This is a common limitation of existing heart models and improving this aspect is the topic of ongoing research. Most likely, the low L-strain is due to the absence of the *atrial kick*, in the computational model. Moreover, no post-systolic shortening, which is an important hallmark of ischemia, is present. Finally, ischemic regions cover full LV segments and are therefore large (cf. Fig. 3). The sensitivity of STE to the extent of the ischemic region, therefore, cannot be tested at present.

In order to register the 2D templates with the 3D model we assumed a textbook definition of the imaging planes given by

This article has been accepted for publication in a future issue of this journal, but has not been fully edited. Content may change prior to final publication. Citation information: DOI 10.1109/TUFFC.2017.2786300, IEEE Transactions on Ultrasonics, Ferroelectrics, and Frequency Control

known rotations along the LV long axis, as illustrated in Fig. 3. Since template recordings were coming from free-hand scans there will be therefore an unavoidable mismatch between the real slice position and the assumed one. An error in the 2D/3D alignment will affect the sampling of the scatter amplitude (hence, the image texture) and of the deformation field (hence, the ground truth values). In this regard, we note that most of the template recordings were coming from a standardization study [6] in which great care was put in reducing all potential sources of variability coming from data acquisition, such as probe positioning. As such, imaging planes are expected to be as much as possible consistent between vendors and in agreement with standard definitions. Most importantly, in our pipeline template recordings are "only" used to transfer a realistic visual texture to the simulation. As such, we are not concerned by a small error in the positioning of the slicing plane as far as the visual appearance of the template recording remains plausible.

The usefulness of the multivendor synthetic dataset presented here is manifold. On one side, it can be used to guide the development of single-vendor speckle tracking solutions. Moreover, it can be used to contrast solutions from different vendors. In this context, we are currently in the process of running a follow up of the initial standardization study [7] where this synthetic dataset is being used to benchmark regional strain measurements from 9 vendors of STE software packages. This includes the 7 manufacturers considered here plus 2 software only companies. Hereto, it is worth noting that data as provided in the open-access database won't be necessarily readable by commercial systems as several of them use a proprietary data format. Further, the provided data can be used to develop more general speckle tracking algorithms not tailored to the images coming from a specific system. Hereto, the availability of realistic synthetic data with associated ground truth displacement could be certainly beneficial in the design of machine-learning based algorithms. Finally, the dataset presented here is based on the same set of E/M simulations which were used in [8] to simulate 3D recordings. The two datasets could therefore be used jointly in order to compare the respective advantages and pitfalls of the 2D and 3D ultrasound technology for strain imaging.

We evaluated the feasibility of the provided database as a bench-marking set for ST algorithms by using one recent technique developed in our lab. Of note, our goal was not to perform a thorough evaluation of a ST algorithm but rather to show that the synthetic datasets could be tracked and that, therefore, could be used for quality assurance of ST techniques. An in deep evaluation of ST techniques remains beyond the scope of this paper. The evaluation showed that the datasets could be tracked with reasonable accuracy. In particular, the performance values obtained are in agreement with what reported in a recent comparison study [10]. Yet, [10] was performed on 3D data and direct comparison is therefore impossible. Of note, we observed a variability in strain accuracy between vendors. Overall, the tested algorithm seemed to perform better on simulated Toshiba images (α closest to 1, highest ρ, low μ, lowest LOA) and slightly worse on simulated Samsung and ESAOTE images (lowest α, lowest ρ, largest LOA). This is a direct consequence of the high variability between image appearance from different vendors and shows the difficulty in developing techniques designed to work on generic systems.

We stress that variability in tracking accuracy between vendors is strictly related to our specific speckle tracking algorithm and therefore must not be generalized. One source of variability might come from the use of sum-of-squared-differences as a data term which, by definition, is intrinsically more sensitive to variations in the changing image appearance between vendors. The use of other feature descriptors more related to image structure, such as mutual information [24] or image phase [25], could reduce such variability. Moreover, it is also important to stress that, although the templates recordings came from commercial systems, all the following steps involved in the generation of the simulated images (scatter map generation, simulation of the RF signals, image reconstruction) were performed with in-house algorithms. All this can introduce a discrepancy between the appearance of images as produced by a specific system and the respective vendor-specific simulations. Overall, no statement about the superiority of the images of one vendor over another can be made, nor this is the purpose of this research.

VI. Conclusion

We presented here what to our knowledge is the largest, most realistic and most diverse ground truth database for 2D STE algorithms available. The database consists of 105 simulated recordings including i) different probe orientation, ii) physiological and pathological contraction patterns and iii) vendor specific image quality. The database can be accessed either from our departmental web-page[4] or directly at http://bit.ly/SyntheticDataQA2DSTE.

Hopefully, this will foster more coordinated and therefore effective and rapid development of the speckle tracking technology. Our work responds to a compelling clinical need to reduce inter-vendor variability between clinically available speckle tracking solutions.

Acknowledgment

The authors would like to thank Prof. Jens-Uwe Voigt and the EACVI/ASE/Industry Standardization Task Force for providing the high quality echocardiographic recordings that were used as "templates" in this study.

References

[1] O. A. Smiseth, H. Torp, A. Opdahl, K. H. Haugaa, and S. Urheim, "Myocardial strain imaging: how useful is it in clinical decision making?" *European Heart Journal*, 2015.

[2] K. Kalam, P. Otahal, and T. H. Marwick, "Prognostic implications of global LV dysfunction: a systematic review and meta-analysis of global longitudinal strain and ejection fraction," *Heart*, 2014.

[3] V. Mor-Avi, R. M. Lang, L. P. Badano, M. Belohlavek, N. M. Cardim, G. Derumeaux, M. Galderisi, T. Marwick, S. F. Nagueh, P. P. Sengupta, R. Sicari, O. A. Smiseth, B. Smulevitz, M. Takeuchi, J. D. Thomas, M. Vannan, J.-U. Voigt, and J. L. Zamorano, "Current and evolving echocardiographic techniques for the quantitative evaluation of cardiac mechanics: ASE/EAE consensus statement on methodology and indications: Endorsed by the japanese society of echocardiography," *Journal of the American Society of Echocardiography*, vol. 24, no. 3, pp. 277 – 313, 2011.

[4] J. D. Thomas and L. P. Badano, "Eacvi-ase-industry initiative to standardize deformation imaging: a brief update from the co-chairs," *European Heart Journal - Cardiovascular Imaging*, vol. 14, no. 11, p. 1039, 2013.

[5] J.-U. Voigt, G. Pedrizzetti, P. Lysyansky, T. H. Marwick, H. Houle, R. Baumann, S. Pedri, Y. Ito, Y. Abe, S. Metz, J. H. Song, J. Hamilton, P. P. Sengupta, T. J. Kolias, J. D'hooge, G. P. Aurigemma, J. D. Thomas, and L. P. Badano, "Definitions for a common standard for 2D speckle tracking echocardiography: consensus document of the eacvi/ase/industry task force to standardize deformation imaging," *European Heart Journal - Cardiovascular Imaging*, 2014.

[6] "Head-to-head comparison of global longitudinal strain measurements among nine different vendors," *Journal of the American Society of Echocardiography*, vol. 28, pp. 1171 – 1181, 2015.

[7] J. D'hooge, D. Barbosa, H. Gao, P. Claus, D. Prater, J. Hamilton, P. Lysyansky, Y. Abe, Y. Ito, H. Houle, S. Pedri, R. Baumann, J. Thomas, and L. P. Badano, "Two-dimensional speckle tracking echocardiography: standardization efforts based on synthetic ultrasound data," *European Heart Journal - Cardiovascular Imaging*, 2015.

[8] M. Alessandrini, M. De Craene, O. Bernard, S. Giffard-Roisin, P. Allain, I. Waechter-Stehle, J. Weese, E. Saloux, H. Delingette, M. Sermesant, and J. D'hooge, "A pipeline for the generation of realistic 3D synthetic echocardiographic sequences: Methodology and open-access database," *IEEE Transactions on Medical Imaging*, vol. 34, no. 7, pp. 1436–1451, July 2015.

[9] S. Marchesseau, H. Delingette, M. Sermesant, M. Sorine, K. Rhode, S. Duckett, C. Rinaldi, R. Razavi, and N. Ayache, "Preliminary specificity study of the bestelclmentsorine electromechanical model of the heart using parameter calibration from medical images," *Journal of the Mechanical Behavior of Biomedical Materials*, vol. 20, pp. 259 – 271, 2013.

[10] M. Alessandrini, B. Heyde, S. Queirs, S. Cygan, M. Zontak, O. Somphone, O. Bernard, M. Sermesant, H. Delingette, D. Barbosa, M. D. Craene, M. O'Donnell, and J. D'hooge, "Detailed evaluation of five 3d speckle tracking algorithms using synthetic echocardiographic recordings," *IEEE Transactions on Medical Imaging*, vol. 35, no. 8, pp. 1915–1926, Aug 2016.

[11] Y. Zhou, S. Giffard-Roisin, M. D. Craene, s. Camarasu-Pop, J. D'hooge, M. Alessandrini, D. Friboulet, M. Sermesant, and O. Bernard, "A framework for the generation of realistic synthetic cardiac ultrasound and magnetic resonance imaging sequences from the same virtual patients," *IEEE Transactions on Medical Imaging*, vol. PP, no. 99, pp. 1–1, 2017.

[12] H. Gao, H. F. Choi, P. Claus, S. Boonen, S. Jaecques, G. Van Lenthe, G. Van der Perre, W. Lauriks, and J. D'hooge, "A fast convolution-based methodology to simulate 2D/3D cardiac ultrasound images," *Ultrasonics, Ferroelectrics and Frequency Control, IEEE Transactions on*, vol. 56, no. 2, pp. 404–409, 2009.

[13] M. Alessandrini, B. Heyde, S. Giffard-Roisin, H. Delingette, M. Sermesant, P. Allain, O. Bernard, M. De Craene, and J. D'hooge, "Generation of ultra-realistic synthetic echocardiographic sequences to facilitate standardization of deformation imaging," in *Biomedical Imaging (ISBI), 2015 IEEE 12th International Symposium on*, April 2015, pp. 756–759.

[14] B. Heyde, R. Jasaityte, D. Barbosa, V. Robesyn, S. Bouchez, P. Wouters, F. Maes, P. Claus, and J. D'hooge, "Elastic image registration versus speckle tracking for 2-d myocardial motion estimation: A direct comparison in vivo," *IEEE Transactions on Medical Imaging*, vol. 32, no. 2, pp. 449–459, Feb 2013.

[15] Q. Fang and D. Boas, "Tetrahedral mesh generation from volumetric binary and grayscale images," in *Biomedical Imaging: From Nano to Macro, 2009. ISBI '09. IEEE International Symposium on*, 2009, pp. 1142–1145.

[16] S. Marchesseau, H. Delingette, M. Sermesant, M. Sorine, K. Rhode, S. Duckett, C. Rinaldi, R. Razavi, and N. Ayache, "Preliminary specificity study of the Bestel-Clement-Sorine electromechanical model of the heart using parameter calibration from medical images," *J Mech Behav Biomed Mater.*, vol. 20, pp. 259–271, 2013.

[17] J. Allard, S. Cotin, F. Faure, P.-J. Bensoussan, F. Poyer, C. Duriez, H. Delingette, and L. Grisoni, "Sofa an open source framework for medical simulation," in *Medicine Meets Virtual Reality 15*, vol. 125, 2017, pp. 13–18.

[18] M. D. Cerqueira, N. J. Weissman, V. Dilsizian, A. K. Jacobs, S. Kaul, W. K. Laskey, D. J. Pennell, J. A. Rumberger, T. Ryan, and M. S. Verani, "Standardized myocardial segmentation and nomenclature for tomographic imaging of the heart: A statement for healthcare professionals from the cardiac imaging committee of the council on clinical cardiology of the american heart association," *Circulation*, vol. 105, no. 4, pp. 539–542, 2002.

[19] A. Myronenko, "Non-rigid image registration regularization, algorithms and applications," Ph.D. dissertation, Oregon Health & Science University, 6 2010.

[20] F. L. Bookstein, "Principal warps: thin-plate splines and the decomposition of deformations," *Pattern Analysis and Machine Intelligence, IEEE Transactions on*, vol. 11, no. 6, pp. 567–585, 1989.

[21] B. Chakraborty, B. Heyde, M. Alessandrini, and J. D'hooge, "Fast myocardial strain estimation from 3d ultrasound through elastic image registration with analytic regularization," in *Proc. SPIE*, vol. 9790, 2016, pp. 979 006–979 006–7.

[22] E. R. DeLong, D. M. DeLong, and D. L. Clarke-Pearson, "Comparing the areas under two or more correlated receiver operating characteristic curves: A nonparametric approach," *Biometrics*, vol. 44, no. 3, pp. 837–845, 1988.

[23] T. Yingchoncharoen, S. Agarwal, Z. Popović, and T. Marwick, "Normal ranges of left ventricular strain: A meta-analysis," *J Am Soc Echocardiogr*, vol. 26, no. 2, pp. 185–91, 2012.

[24] H. V. T. K. L. W. E. David Mattes, David R. Haynor, "Nonrigid multimodality image registration," vol. 4322, 2001, pp. 4322 – 4322 – 12. [Online]. Available: http://dx.doi.org/10.1117/12.431046

[25] M. Alessandrini, H. Liebgott, D. Barbosa, and O. Bernard, "Monogenic phase based optical flow computation for myocardial motion analysis in 3D echocardiography," in *Statistical Atlases and Computational Models of the Heart. Imaging and Modelling Challenges*, ser. Lecture Notes in Computer Science, O. Camara, T. Mansi, M. Pop, K. Rhode, M. Sermesant, and A. Young, Eds. Springer Berlin Heidelberg, 2013, vol. 7746, pp. 159–168.